H. -J. Wang[1], R. Merz[1], S. Yang[2], L. Tarasova[1] and S. Basso[1]

[1]Department of Catchment Hydrology, Helmholtz Centre for Environmental Research – UFZ, Halle (Saale), Germany,

[2]Department of Aquatic Ecosystem Analysis, Helmholtz Centre for Environmental Research – UFZ, Magdeburg, Germany

Corresponding author: Hsing-Jui Wang (hsing-jui.wang@ufz.de)

Key Points:

- Increasing spatial variability of rainfall determines heavier streamflow tails only beyond a certain increase threshold.
- Small and elongated catchments are less resilient to increasing spatial variability of rainfall.
- Daily records of rainfall and streamflow for a large set of catchments in Germany confirm simulations.

Abstract

Flow events with low frequency often cause severe damages, especially if their magnitudes are higher than suggested by historical observations. Heavier right tail of streamflow distribution indicates the increasing probability of high flows. In this paper, we investigate the role played by spatially variable rainfall for enhancing the tail heaviness of streamflow distributions. We synthetically generated a wide range of spatially variable rainfall inputs and fed them to a continuous probabilistic model of the catchment water transport to simulate streamflow in five catchments with distinct areas and geomorphological properties. Meanwhile, we used a comparable approach to analyze rainfall and runoff records from 175 German catchments. We identified the effects of spatially variable rainfall on tails of streamflow distributions from both simulation scenarios and data analyses. Our results show that the tail of streamflow distribution becomes heavier with increasing spatial rainfall variability only beyond a certain threshold. This finding indicates a capability of catchments to buffer growing heterogeneities of rainfall, which we term catchment resilience to increasing spatial rainfall variability. The analyses suggest that the runoff routing process controls this property. In fact, both small and elongated catchments are less resilient to increasing spatial rainfall variability due to their intrinsic runoff routing characteristics. We show the links between spatial rainfall characteristics and catchment geometry and the possible occurrence of high flows. The data analyses we performed on a large set of case studies confirm the simulation results and provide confidence for the transferability of these findings.

Plain Language Summary

High flow events often cause severe damages when they occur unexpectedly, i.e., more often and with larger magnitudes than suggested by historical observations and common experience. This is usually the case in catchments with

frequency distributions of streamflow which are heavy-tailed. In these cases, the possibility that any large flow magnitude will occur cannot be neglected. However, a proper assessment of the right tail of streamflow distributions solely based on limited data records is indeed difficult and might lead to an erroneous estimation of the underlying hazard. In this study we investigate if spatially heterogeneous rainfall enhances heavy-tailed streamflow distributions, i.e., whether it increases the probability of very high flow events. This is especially important because a considerable increase in the spatial variability of rainfall may appear due to global warming. We found that catchments are able to buffer increasing spatial rainfall variability up to a certain point. We call this property catchment resilience to spatial rainfall variability. We also found that the catchment resilience is related to the size and shape of river basins. The results have implications for the evaluation of the impacts of spatial heterogeneous rainfall on the hazard of high flows in different catchments.

1 Introduction

Extreme streamflow events often occurred unexpectedly and caused severe human safety issues and economic devastation. The extremeness of streamflow is referred to its low frequency and high magnitude among the historical observations for certain regions, which is commonly shown in the heavy tail of a streamflow distribution. Heavy-tailed distributions are used to be defined as: extreme values are more likely to occur than would be predicted by distributions that have exponential asymptotic behavior (El Adlouni, 2008). This sizable probability of the occurrence of extreme streamflow is therefore a marking of enhanced flood hazard in respect of flow frequency and magnitude. Heavy-tailed streamflow occurs in many catchments around the world (Bowers et al., 2012; Katz et al., 2002). It causes severe problems as humans tend to underestimate flood risk in heavy-tailed catchments (Taleb, 2007). Hence it is of the utmost importance to understand hydrological causes of heavy tails in streamflow distributions, which is also important for catchments with observed streamflow records not long enough to derive heavy tail behavior from historical data (Wietzke et al, 2020) and in ungauged catchments (Yokoo & Sivapalan, 2011). Moreover, investigating the role of emerging heavy tails in streamflow distributions is a useful tool to link modifications of extreme streamflow to changes in climate conditions (Basso et al., 2015).

Some potential variables of heavy-tailed streamflow distributions have been suggested in previous studies: e.g., drier catchments (Sivapalan et al., 2005), smaller catchments (Villarini & Smith, 2010), non-linear runoff response to precipitation (Basso et al., 2015; Gioia et al., 2008). Yet the generation processes and exact causing factors to heavy-tailed streamflow distributions are still poorly understood. Regarding causing factors of extreme streamflows, rainfall is often considered to be an important issue (e.g., Arnell & Gosling, 2014; Bracken et al., 2008; Wasko & Sharma, 2017). Spatial rainfall variability has been proved as non-negligible to accurate streamflow prediction (e.g., Singh, 1997; Zhao et al., 2013; Zoccatelli et al., 2011) and is likely to become more critical to eval-

uate impacts of climate changes on extreme streamflow events. The increasing trend in the occurrence of localized and extreme rainfall events has been found under global warming conditions (Donat et al., 2016; Li et al., 2019; Myhre et al., 2019; Pendergrass, 2018), hence a considerable rise in spatial rainfall variability may be an expected consequence. However, traditionally, the focus of the effects of spatially variable rainfall on streamflow has always been the variability of a single rainfall storm or the magnitude of the resulting peak discharge (Borga et al., 2007; Lu et al., 2017; Paschalis et al., 2014; Viglione et al., 2010). Few researchers have addressed the issue of the effects of continuous spatially variable rainfall on streamflow distributions (which also indicate the flood hazards based on the variation between low and high flows instead of only peak flows). Furthermore, long-term streamflow response (e.g., cumulative streamflow distributions) to rainfall is linked with multiple hydrological processes and complex interactions in between catchment units. There is still some controversy surrounding concerning the impacts of heterogeneous rainfall on streamflow due to variable climate conditions (Viglione et al., 2010; Zhao et al., 2013), catchment sizes (Merz & Blöschl, 2009; Zhu et al., 2018), or the heterogeneities from other catchment attributes (Harman et al., 2009; Rogger et al., 2012; Struthers & Sivapalan, 2007). Hence, it remains a great challenge for hydrologists to understand the linkages between the changing characteristics of rainfall and high flows. Sharma et al. (2018) suggested more attention to the complexity of the relations between entire variables in river basins is deserving. They also pointed out one of the foremost issues, which is still missing, is the relations between catchment size, catchment geometry, and storm characteristics (e.g., extent, duration, intensity). In the meanwhile, providing a corresponding data validation to modeling results is challenging. A general investigation of the effects of spatial rainfall variability from both simulation scenarios and data analyses is needed.

In this study, we start from two research questions: (1) what is the role of the spatial rainfall variability on heavier-tailed streamflow distributions, and (2) does this role be modified due to different catchment sizes and shapes. We aim to investigate the research questions using both simulation scenarios and data analyses. This paper is organized as follows: Section 2 describes the study catchments and the hydrological data, Section 3 describes the generation of spatially variable rainfall, the continuous probabilistic model of the hydrologic response, the indices of tail heaviness and catchment characteristics, and the approaches for data analyses. In Section 4, results and discussion of the effects of spatial rainfall variability on streamflow-distribution tail heaviness are described under different catchment sizes and shapes both from simulation scenarios and data analyses. The main conclusions of the paper are summarized in Section 5.

2 Data

The study is based on daily precipitation and streamflow observations for a set of 175 German catchments taken from Tarasova et al. (2018). Catchments influenced by large reservoirs or control gates (Lehner et al., 2011) and affected by

visible anthropogenic streamflow disturbances are disregarded. The catchment areas vary from 36 to 23,700 km^2, with a median value of 688 km^2.

The length of daily streamflow and rainfall time series range between 37 and 63 years (between 1951 and 2013) with a median value of 61 years. We computed the specific (i.e., per unit catchment area) streamflow for all catchments and used the term 'streamflow' to denote it throughout this paper. Rainfall time series for each catchment was derived from the Regionalisierung der Niederschlaghöhen (REGNIE) dataset, which is a 1 km^2 resolution rainfall field interpolated from point observations through multiple regression, provided by the German Weather Service (Rauthe et al., 2013). The analysis was restricted to the summer periods to avoid bias from snow melting, which is not taken into account in the adopted modeling framework. Summer season was identified as June to August, as suggested by Beurton and Thieken (2009) for German catchments. Daily temperature time series in the considered catchments were generated from the German Weather Service observations by means of external drift kriging, using elevation as an explanatory variable (Zink et al., 2017), and here applied for the estimation of potential evapotranspiration by means of the Thornthwaite (1948) equation.

All 175 catchments were used in the data analysis and five catchments out of them were selected for scenario simulations (Figure 1). The Delme river basin at Holzkamp (small size), the Ilm river basin at Niedertrebra (medium size), and the Amper river basin at Inkofen (large size) form the first group of basins used in the simulations for they have various catchment sizes while their drainage densities and elongation ratios are similar. The Ilm river basin at Niedertrebra (more elongated), the Innerste river basin at Heinde (less elongated), and the Unstrut river basin at Erfurt-Moebisburg (circular) form the second group of basins used in simulations for they have various catchment shapes while their drainage densities and sizes are similar (see supporting information Table S1 for details).

A 100-m resolution digital elevation model (DEM) retrieved from the Shuttle Radar Topography Mission (SRTM) was used to generate the river networks of the five select catchments. River networks were determined by means of the Arc Hydro tools with the recommended threshold (i.e., 1%) for stream determination (ESRI, 2009). Catchment units were defined as the drainage area comprised between neighboring nodes of the river network, or by the area draining to the uppermost nodes.

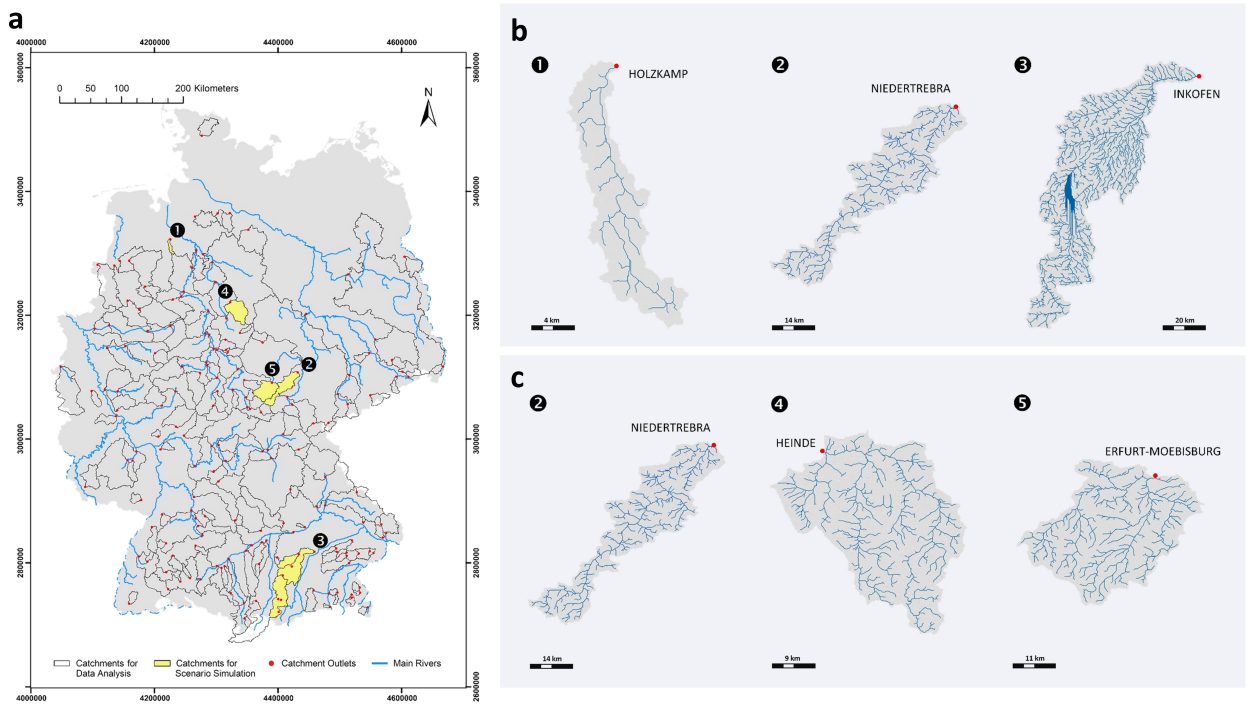

Figure 1. Study catchments. (A) Study catchments on the map of Germany. Black contours show the boundaries of 175 catchments used for data analyses. The yellow shaded areas labeled with numbers corresponding to panels b and c indicate the five catchments used for scenario simulation. (B) Catchments selected for analyzing the effects of catchment size. The river networks and drainage areas of the Delme river basin at Holzkamp (), the Ilm river basin at Niedertrebra (), and the Amper river basin at Inkofen. (C) Catchments selected for analyzing the effects of catchment shape. The river networks and drainage areas of the Ilm river basin at Niedertrebra (), the Innerste river basin at Heinde (), and the Unstrut river basin at Erfurt-Moebisburg ().

3 Methods

3.1 Generation of Spatially Variable Rainfall

We generated synthetic spatially variable rainfall on each catchment for each day by randomly extracting values from a preassigned probability distribution (alike Ayalew et al., 2014), which were then allocated to each catchment unit. The Gamma distribution was identified (from the REGNIE rainfall fields) as the most suitable distribution to represent the observed spatial variability of rainfall within five select catchments (see supporting information Text S1 and Figure S1) and hence adopted here. We considered two scenarios (stationary and nonstationary; Figure 2) to distinguish between effects on the tail of the streamflow probability distribution caused by either constant (i.e., stationary)

spatial rainfall variability for all events (postulated to have duration of one day) or variable (i.e., nonstationary) spatial rainfall variability between all events of the time series.

Figure 2 exemplary illustrates differences among spatially uniform and variable rainfall in the stationary and nonstationary scenarios. In the uniform case (Figure 2a) the synthetic rainfall field is uniform in space with a rainfall depth equal to the catchment average rainfall depth of that day derived from REGNIE. In the stationary scenario (Figure 2b) every day exhibits different spatial rainfall patterns, while the spatial variability (measured as coefficient of variation of rainfall) is constant for all days. Again, for each day, the catchment average synthetic rainfall depth equals the observed value. In contrast, the spatial variability changes day by day in the nonstationary scenario, with catchment average synthetic rainfall depth each time equals to the catchment average calculated from REGNIE (Figure 2c).

To obtain these scenarios the shape parameter of the Gamma distribution was either fixed for all days (stationary scenarios) or allowed to vary randomly within a specified range (nonstationary scenarios). The scale parameter was then determined by setting the mean of the Gamma distribution equal to the average observed daily rainfall.

To obtain stationary rainfall fields we fixed the shape parameter of the Gamma distribution, k, for all days in the time series. To generate different degrees of rainfall spatial variability we imposed fifty-two different values of k between 10^3 and 10^{-4} (see supporting information Table S2), which resulted in a wide range of variabilities from extremely low (near to homogeneous, with the largest k) to extremely high (when the smallest k are utilized).

For the nonstationary rainfall fields, the shape parameter k of the Gamma distribution was changed day by day. In particular, we allowed for it to randomly fluctuate around a central value k_0 within a specified range *(-b,b)*. We generated rainfall fields characterized by low to high degrees of nonstationarity by varying the width of this range and assigning to b twenty different values between $0.05k_0$ and k_0. We set k_0=10^{-1}, i.e., an intermediate value among those analyzed for k in the stationary scenario (see supporting information Table S3). With this approach we generated variations of the spatial variability across events while controlling the average spatial variability within events to highlight effects due to nonstationarity of spatial rainfall variability only.

For each of the described scenarios (stationary vs nonstationary), each degree of spatial variability (i.e., each k value) in the stationary case and each degree of nonstationarity (i.e., each $k_0 \pm b$), a hundred stochastic realizations were generated to assess the uncertainty of the results.

We adopted three distinct indices (Equation 1 to 3) to evaluate the degree of variability of the synthetically generated spatial rainfall fields. The first index is the coefficient of variation in space (CV_{space}) of the rainfall depth assigned to all catchment units in each day, which we termed $CV_{space,t}$ for day t:

$$CV_{space,\ t} = \frac{\sqrt{\frac{1}{U}\sum_{u=1}^{U}\left(d_{u,t}-\overline{d_t}\right)^2}}{\overline{d_t}}$$

(1)

where $d_{u,t}$ [mm] is rainfall depth at catchment unit u on day t, $\overline{d_t}$ is the spatial mean of rainfall on day t, U is the total number of catchment units.

The second index is the temporal mean of the first index, which characterizes the average spatial variability of rainfall across all wet days (i.e., days with rainfall > 0) of the time series. It is computed as:

$$\mathrm{CV_{in}} = \frac{1}{T}\sum_{t=1}^{T}\mathrm{CV}_{space,\ t}$$

(2)

where T is the total number of wet days in the rainfall time series of a catchment.

The third index is the temporal coefficient of variation of the first index, which represents the fluctuation of the spatial rainfall variability from one day to the other. It is calculated as the coefficient of variation of CV_{space} across all wet days (i.e., days with rainfall > 0) in the time series:

$$\mathrm{CV_{cross}} = \frac{\sqrt{\frac{1}{T}\sum_{t=1}^{T}\left[\mathrm{CV_{space}}-\mathrm{CV_{in}}\right]^2}}{\mathrm{CV_{in}}}$$

(3)

Note that for the case of uniform rainfall, both CV_{in} and CV_{cross} are equal to zero. In the stationary scenario CV_{cross} is always equal to zero and different values of CV_{in} are investigated, whereas CV_{cross} is different from zero in the non-stationary scenario.

The approach here applied to generate spatially variable rainfall fields is inspired by Ayalew et al. (2014). We recognize that such an approach does not take into account the spatial organization of rainfall due to orographic or atmospheric factors, and that more sophisticated methods to generate spatial rainfall fields exist (e.g., Papalexiou & Serinaldi, 2020). However, the method was chosen because it provides some advantages in the context of the present study, namely, it avoids potential impacts from the actual spatial organization of rainfall and its interaction with different catchment response times (which are here fully explored by means of random realizations of the defined processes) to instead highlight the effect of the spatial variability of rainfall only, which is the scope of this study. Moreover, using synthetic rainfall instead of the observed spatial patterns enables investigating a wider range of variability than the one that has been observed. Finally, such an approach allows for isolating and analyzing separately the role played by spatial rainfall variability occurring within the same

rainfall event or by changes of spatial variability across events, thus enabling an understanding of the effect of each of these components.

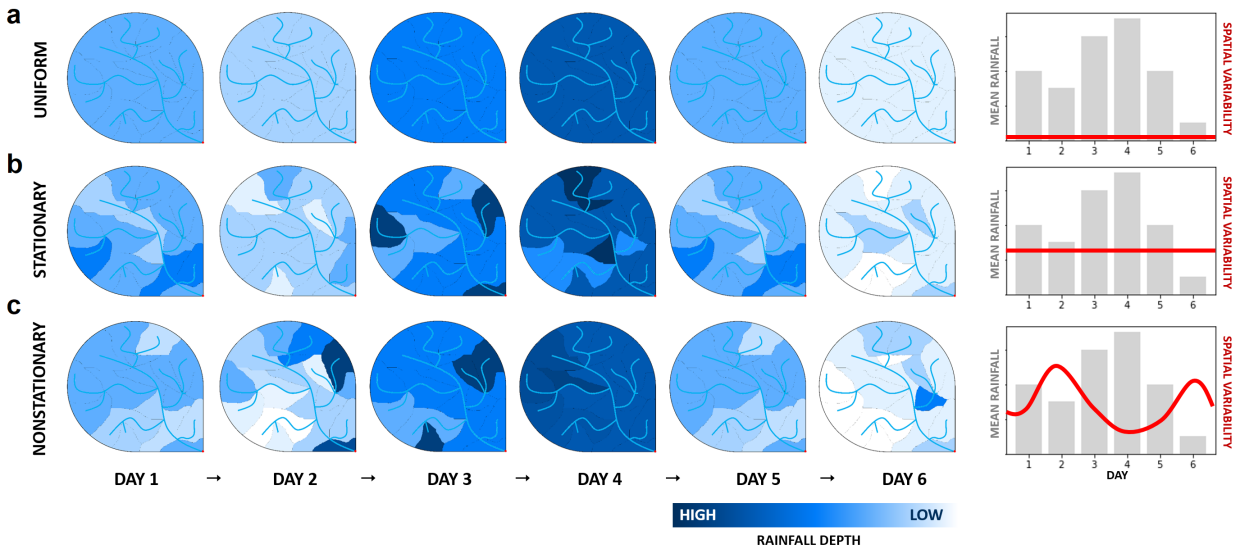

Figure 2. Schematic diagram of spatial rainfall scenarios. All three panels have the same series of mean daily rainfall depth but various spatial variability of rainfall, which is measured through its coefficient of variation in space. (A) Rainfall uniformly distributed in space (i.e., the spatial variability is zero). (B) Stationary spatial variability of rainfall, i.e., constant spatial coefficient of variation across days. (C) Non-stationary spatial variability of rainfall, i.e., variable spatial coefficient of variation day by day.

3.2 Continuous Probabilistic Model of the Hydrologic Response

We used a well-established probabilistic model of the water transport at the catchment scale (D'Odorico & Rigon, 2003; Nic tina et al., 2008; Park & Seo, 2014; Rigon et al., 2016; Rinaldo & Rodriguez-Iturbe, 1996; Rinaldo et al., 2006; Rodriguez-Iturbe & Valdes, 1979) to simulate streamflow at the outlet of catchments forced by spatially variable rainfall fields. The model accounts for three key components (see supporting information Figure S2): (1) the soil water balance in hillslopes, (2) the probability distributions of transit times in the hillslopes of catchment units, here assumed to be stationary in time, and (3) the response time distribution in channels derived from a geomorphological analysis of the river network.

The first component represents the water balance among rainfall inputs, evapotranspiration, and leaching to subsurface flow in each catchment unit:

$$\frac{dV(t)}{\mathrm{dt}} = [I(t) - ET(t) - L(t)] \cdot A$$

(4)

where V is the water storage in the root zone [mm^3], I is the infiltrated rainfall depth [mm], ET is the evapotranspiration [mm], L is the leaching from the storage to subsurface flow [mm], A is the area of the catchment unit [mm^2], and t is the daily time interval [day]. The water storage V is then used to calculate soil moisture (SM) as:

$$\mathrm{SM}(t) = \frac{V(t)}{m \cdot Z \cdot A}$$

(5)

where m is the soil porosity [-] and Z is the depth of the root zone [mm].

In each catchment unit at time t, hydrological processes were further distinguished as the responses in unsaturated (A_{us}(t)) and saturated areas (A_s(t)). We estimated the fraction of saturated area to total area as a power-law function of soil moisture (Kirkby, 1975). In unsaturated areas all the rainfall infiltrates (i.e., $I(t) = P(t) \cdot \frac{A_{\mathrm{us}}(t)}{A}$, where P is the rainfall depth [mm]) whereas in saturated areas no infiltration occurs and rainfall becomes surface runoff, and evapotranspiration equals its potential value estimated according to Thornthwaite (1948). Evapotranspiration in unsaturated areas is instead considered as a linear function of the soil moisture between the wilting point (set equal to 0.05; Ács et al., 2010) and a critical point when the water available for this process is non-limiting. Leaching of water to subsurface flow paths takes place in both unsaturated and saturated areas, and is computed as a power-law function of soil moisture multiplied by a coefficient which is equal to the hydraulic conductivity (Clapp & Hornberger, 1978).

Transit times in the hillslopes of catchment units (i.e., the second key component of the model) were assumed to be exponentially distributed. Distinct distributions were considered for the surface ($f_{sup,h}$) and subsurface ($f_{sub,h}$) flow paths. Their respective parameters were determined through a power law relationship with the size of the catchment unit (Boyd, 1978; D'Odorico & Rigon, 2003; Nic tina et al., 2008). All water particles in the source hillslopes were assumed to flow towards the lower node of each catchment unit.

The third component, namely the response time distributions in river networks (f_n), was instead derived from the width function of the catchment unit which explicitly considered the length of the pathway from the lower node of the catchment unit to the catchment outlet and the integration of the simplified parabolic model of de Saint Venant equation with suitable boundary conditions (Rinaldo et al., 1991; Rinaldo & Rodriguez-Iturbe, 1996).

The response time distribution of a catchment unit was finally obtained by convoluting f_n with either $f_{sup,h}$ or $f_{sub,h}$ for respectively surface and subsurface flow. Streamflow generated from a catchment unit was finally simulated as the

convolution of the runoff (i.e., the outcome of the first component) and the response time distribution (i.e., the outcome of the second and third components). Both superficial flow and subsurface flow were simulated at the outlet from each sub catchment and the integral of surface and subsurface contributions from all catchment units formed the total streamflow at the catchment outlet.

The model was calibrated on the observed streamflow series at the catchment outlet by using spatially uniform rainfall inputs. We used the shuffled complex evolution algorithm by applying a statistical parameter optimization tool of Python, SPOTPY (Houska et al., 2015) for the optimization of parameters.

3.3 Indices of Tail Heaviness

We applied two distinct approaches to evaluate the relative and absolute heaviness of the tails of streamflow probability distributions. First, we quantified the relative heaviness of the upper tail of streamflow distributions resulting from spatially variable rainfall inputs with respect to the heaviness of the distribution obtained with uniform rainfall (see section 3.3.1). Second, we further inspected if the tails of the former distributions are heavy in absolute terms, by evaluating the plausibility of a power law distribution to represent them (see section 3.3.2).

3.3.1 Relative Tail Heaviness of Upper-Tailed Slope

We used the slope S of the upper tail of the exceedance probability distribution of normalized daily streamflow (normalized by the mean value of the streamflow time series) represented in a double logarithmic plot (see supporting information Figure S3) as an index of tail behavior, similarly to Nerantzaki and Papalexiou (2019) and Mushtaq et al. (2022). This is defined as:

$$S = \left| \frac{\log(0.01) - \log(0.1)}{\log\left(x_{0.01}\right) - \log(x_{0.1})} \right| \quad (6)$$

where $x_{0.01}$ and $x_{0.1}$ are the values of the normalized streamflow corresponding to the exceedance probabilities of 0.01 and 0.1.

We normalized S with the slope of the reference case, S_0, here represented by the streamflow distribution obtained from the uniform rainfall case. Since the tail heaviness is proportional to the inverse of the tail slope, the index of relative tail heaviness H is therefore:

$$H = \frac{S_0}{S} \quad (7)$$

Accordingly, $H > 1$ indicates a streamflow distribution with a tail which is heavier than the one of the distribution obtained with uniform rainfall, whereas

$H < 1$ labels a distribution with a lighter tail than the distribution obtained with uniform rainfall (see supporting information Figure S3).

3.3.2 Suitability of Best-Fit Power Law Distribution

Power law distributions are a type of heavy-tailed distributions (i.e., distributions with tails heavier than exponential ones) with special relevance as they occur in a wide range of natural and man-made phenomena (Newman, 2005). In particular, power law distributed variables can assume values very far from their mean. For the case of streamflow, this translates into an unneglectable chance of occurrence of very large flows and therefore in the possible occurrence of extreme floods.

For this reason, we investigated the possible emergence of power law distribution (i.e., distributions which are heavy-tailed in an absolute sense) as a result of spatially variable rainfall inputs. To this purpose, we applied a robust statistical framework (Clauset et al., 2009) to identify power law distributions in empirical data. The range of the tail was determined as the streamflow above a lower boundary value which made the probability distribution of the streamflow above the boundary and the best-fit power-law model as similar as possible. Kolmogorov-Smirnov statistic was applied to quantify the distance between two probability distributions (i.e., the cumulative distribution function of data and the fitted power-law model). The associated p-value was used to evaluate whether the power law is a plausible fit to the data.

3.4 Topological Characteristics of Catchments

We applied classical indices to quantify some topological characteristics of our study catchments that may be relevant for their hydrological responses, and used them to compare the behaviors of catchments.

3.4.1 Drainage Density

Drainage density (D_d) is defined as the total length of the channel in a catchment divided by the catchment area (Horton, 1932):

$$D_d = \frac{\sum l}{A} \quad (8)$$

where l is the length of a channel segment in a river network and A is the total area of the catchment. It represents the average length of channel per unit catchment area, a feature which is often related to possibilities for infiltration and permeability of a catchment (Adhikari, 2020; Nag & Chakraborty, 2003).

3.4.2 Elongation Ratio

Several dimensionless indices have been proposed to quantify the shape of catchments. One of the most well known indices is the elongation ratio, R_e (Shumm,

1956). It takes into account the total area of the catchment (A) and the longest distance from the catchment boundary to the outlet (L) to evaluate the catchment shape. This is defined as:

$$R_e = \frac{2\sqrt{A}}{L\sqrt{\pi}} \quad (9)$$

where is Archimedes' constant. The elongation ratio has been found to vary from 0.6 to 1.0 in a wide set of catchments with various climatic and geologic characteristics (Strahler, 1964). Catchment shapes are generally distinguished according to the following classification: circular (0.9−1.0), oval (0.8−0.9), less elongated (0.7−0.8), elongated (0.5−0.7), and more elongated (< 0.5) (Withanage et al., 2014).

3.5 Approaches for Data Analyses

The relationship between spatial rainfall variability and tail heaviness of the streamflow distribution was also investigated based on observed rainfall-runoff events from 175 catchments across Germany. In this case we applied the same index of average spatial rainfall variability (i.e., CV_{in}), index of relative tail heaviness (i.e., H), and suitability of power law distributions for the data. An interpolated gridded rainfall dataset (see section 2) was used to identify the rainfall fields.

Rainfall-runoff events were separated from the continuous recorded series using the approach proposed by Tarasova et al. (2018). The spatial variability of rainfall for each runoff event (i.e., CV_{space}) was computed based on the spatial rainfall pattern of the total event rainfall (Tarasova et al., 2018).

To highlight the streamflow responses from different spatial rainfall variability, we sorted the rainfall-runoff events based on their CV_{space} value. Events were then binned into groups of 100 members from low to high spatial rainfall variability, which formed a bin with a certain value of spatial rainfall variability equal to the mean CV_{space} of the 100 events (i.e., CV_{in}). Events with the largest spatial rainfall variability were considered as a separate category if their number was equal or above 50, otherwise they were included in the prior category.

The streamflow distribution and its tail heaviness were calculated by using the peak values of the 100 runoff events included in each bin. Due to different numbers of events for catchments in our data set, 5 to 17 bins (median: 12 bins) were determined in one catchment for analyzing the relationship of spatial rainfall variability and tail heaviness of streamflow. The number of events per bin was decided as a tradeoff between the needs of obtaining reliable estimates of tail heaviness (which improve with the number of events per bin) and a suitable representation of the relationship between spatial rainfall variability and tail heaviness (which instead requires a certain number of bins).

Linear regression between the tail heaviness of streamflow distributions and the corresponding average spatial rainfall variability was performed and the Pearson correlation coefficient and the Wald Test with t-distribution were computed by means of the scipy.stats.linregress tool of SciPy v1.7.1.

4 Results and Discussions

4.1 Effects of spatial rainfall variability on tail heaviness of streamflow distributions

An exemplary illustration of the effects of increasing spatial rainfall variability (CV_{in}, i.e., in a stationary scenario) from modeling results is shown in Figure 3 for the Ilm river at the gauging station of Niedertrebra. The red shaded area identifies cases with heavier tails than in the case of uniform rainfall. The black dots and tendency line express the mean tail heaviness among hundred realizations performed for each degree of spatial rainfall variability. They indicate that the tail heaviness of the streamflow distribution increases only beyond a certain threshold of spatial rainfall variability, which is equal to $CV_{in} = 4.7$ for the gauging station of Niedertrebra. To quantify this threshold, we developed and applied an approach which considers the statistical significance, the correlation coefficient, and the relation of data. It is detailed in the supporting information Text S2.

On the left-hand side of this threshold the spatial rainfall variability produces both heavier and lighter tails than in the case of uniform rainfall. This is an outcome of heavier rainfall occurring either in downstream or upstream parts of the catchment for a single considered stochastic realization. The range spanned by values of the tail heaviness increases along with the increase of spatial rainfall variability, which indicates that the specific rainfall patterns have an increasing influence on the observed tail heaviness with increasing heterogeneity of rainfall. The effect of heterogeneous rainfall is also modulated by soil moisture dynamics in each catchment unit. Viglione et al. (2010) suggested that the spatial heterogeneity of rainfall was more impactful in regions affected by saturation-excess than infiltration-excess phenomena. In line with the latter study, also Zhao et al. (2013) found that the spatial variability of soil moisture was produced when the spatial rainfall variability increased in both wet and dry conditions, while the soil moisture showed stronger sensitivity to rainfall in wet conditions (i.e., saturation-excess dominance) than in dry conditions (i.e., infiltration-excess dominance). In general, spatially variable rainfall produces heterogeneity in the soil moisture and thus generates more opportunities of partial saturation excess (i.e., when rainfall fall on saturated catchment units) than in the uniform rainfall case. This leads to streamflow distributions with heavier tails. However other attenuating effects, such as runoff routing through the river network, may average out the effects of these heterogeneities on the hydrograph (Merz & Blöschl, 2009). On average, the tail heaviness of streamflow distributions for relatively smaller values of spatial rainfall variability does not significantly differ from the case with uniform rainfall due to these interactions. Conversely, for higher spatial rainfall variability a strong positive correlation between spatial

rainfall variability and increased tail heaviness exists. This is likely due to the increasing dominant effect of surface flow generated from partially saturated area in condition of high spatial heterogeneity.

Red dots indicate realizations for which the streamflow distributions are plausibly represented by means of power laws. Large amounts of red dots (i.e., realizations for which the streamflow distributions are plausibly represented by means of power laws) are visible for high spatial rainfall variability. This indicates that, besides increasing the tail heaviness of streamflow distributions, highly heterogeneous rainfall also gives rise to distributions that are heavy in an absolute sense, which have an unneglectable probability of the occurrence of extreme flow events.

By identifying the distinct responses of tail heaviness to the increase of spatial rainfall variability below and beyond a certain threshold, our findings suggest the existence of resilience of catchments to increasingly variable spatial rainfall. We used here the term 'catchment resilience' to indicate the capability of a catchment to buffer increasingly variable spatial rainfall patterns with reducing changes in the tail heaviness of its streamflow distribution, which is an indicator of the probability of occurrence of extreme flow events. This property may have important implications for the assessment of the peril of floods under climate change, which is predicted to increase the spatial heterogeneity of rainfall both locally and globally (Donat et al., 2016; Donat et al., 2019; Li et al., 2019; Myhre et al., 2019; Pendergrass, 2018).

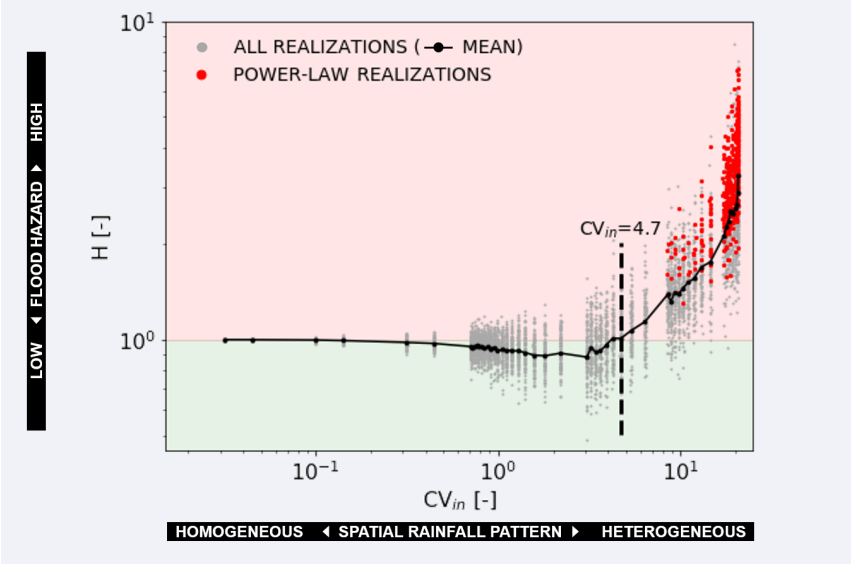

Figure 3. Effects of increasing spatial rainfall variability (CV_{in}) on the tail heaviness of the streamflow distribution of the Ilm river at the gauging station of Niedertrebra. The red shaded area indicates heavier-tailed streamflow distributions with respect to the uniform rainfall case, whereas the green shaded

area indicates lighter-tailed streamflow distributions. For each value of CV_{in} hundred different realizations of spatial rainfall patterns on the catchment characterized by the same spatial rainfall variability are displayed with gray dots. The mean values of the tail heaviness among hundred results for each CV_{in} are marked in black and linked with a tendency line. The black-dash line indicates the identified threshold of spatial rainfall variability beyond which the tail heaviness of the streamflow-distribution increases (see supporting information Text S2). Red dots indicate realizations for which the streamflow distributions are not simply relatively heavier than in the uniform rainfall case, but heavy in an absolute sense as they are plausibly fit by power law distributions.

4.2 Effects of Catchment Size and Shape

We analyzed the effects of a wide range of spatial rainfall variability in 5 select catchments with various sizes and shapes to investigate whether these catchment characteristics affect their resilience to increasing spatial rainfall variability. Figure 4a shows the effects of increasing spatial rainfall variability on the tail heaviness of streamflow distributions in the Delme river basin at Holzkamp (82 km^2), Ilm river basin at Niedertrebra (887 km^2), and Amper river basin at Inkofen (2814 km^2). Results are plotted together to compare the responses in catchments with different sizes. To highlight the effects of catchment size, we selected catchments which are comparable to what concerns other potentially influencing factors, such as their shapes. All of them are therefore elongated catchments with elongation ratio $R_e < 0.5$ and have small drainage density (i.e., $D_d < 1$).

All three catchments show increasing tail heaviness of streamflow distributions as a result of increasing spatial rainfall variability. However, the minimum value of spatial rainfall variability for which an effect arises varies, indicating different degrees of resilience in small and large catchments. The effect becomes visible at a lower rainfall variability in the smallest catchment (82 km^2). The tail heaviness is higher in this case than for the other two catchments for all values of rainfall variability. This suggests the least resilience to spatial rainfall variability in the small catchment. The effect instead arises for similar values of spatial rainfall variability for medium and large catchments. However, the tail heaviness increases quicker in the former, thus suggesting higher resilience of large catchments to increasing spatial variability of rainfall.

As we discussed in the previous section, the runoff routing may balance the impacts of partial saturation excess from catchment units caused by the spatially heterogeneous rainfall. Although partial saturation excess may increase fast flow, the increase would be contrasted by a delayed response if it occurs at upstream catchment units (i.e., more remote region from the outlet). This contrasting capability of a catchment is linked to the runoff routing distance distribution of its river network. In general, the longer the distance the larger the capacity would be. Figure 4b shows the cumulative distribution functions (CDF) of the runoff routing distance of the three catchments. It is clear that the small catchment has the narrowest spread of the distribution (i.e., all catchment

units are near the outlet compared to the other two larger catchments) and therefore has the least resilience. Figure 4c shows the CDFs of the runoff routing distance normalized with respect to the longest distance in each river network, which allows for better evaluating the relative distributions of the distance in the catchments. The black dashed line is the 45-degree line. Both small and medium catchments' CDFs are closed to uniform distributions (i.e., the S-Curves are closed to straight lines) whereas the large catchment's CDF is likely an asymmetrical distribution (i.e., the area below the 45-degree line is different with the above). When the runoff routing distance distribution is a uniform distribution, the routing effects from the fast and delayed response are equal and balance each other; when the distribution is asymmetrical, instead, the routing effects are inequivalent from the fast and delayed response. For the case in Figure 4c, the large catchment displays a right skew distribution (i.e., there is greater area above the 45-degree line than below for the blue S-curve) which indicates a stronger overall routing effect to partial saturation excess. This may be an additional reason for the large catchment responses being slower than the medium catchment in Figure 4a.

Some studies suggested that small catchments are subject to higher flood risk than large catchments due to higher possibilities of a large extension of saturated areas (e.g., Darras et al., 2015; Rogger et al., 2012; Zhu et al., 2018). Unfortunately, the spatial rainfall variability was essentially not unified (e.g., rainfall is generally more spatially uniform in small catchments than large catchments) in those cases, hence the difference of the hydrological responses in a small and a large catchments to a given spatial rainfall variability can hardly be assessed. Gupta & Waymir (1998) proposed a power-law scaling of peak discharge resulting from a single rainfall event (which is one of the main contributors to the heavy tail of a streamflow distribution) with drainage area and showed that the dominant factors of the scaling was the rainfall variability at smaller catchments and were the river network structure and flow dynamics at larger catchments. Others suggested the attenuating effects of the river networks decreased the importance of spatial and temporal rainfall variability at larger catchment scales (Marchi et al., 2010; Menabde et al., 2001; Woltemade & Potter, 1994). In agreement with these studies we show stronger attenuation of spatially heterogeneous rainfall from river networks of larger than smaller catchments.

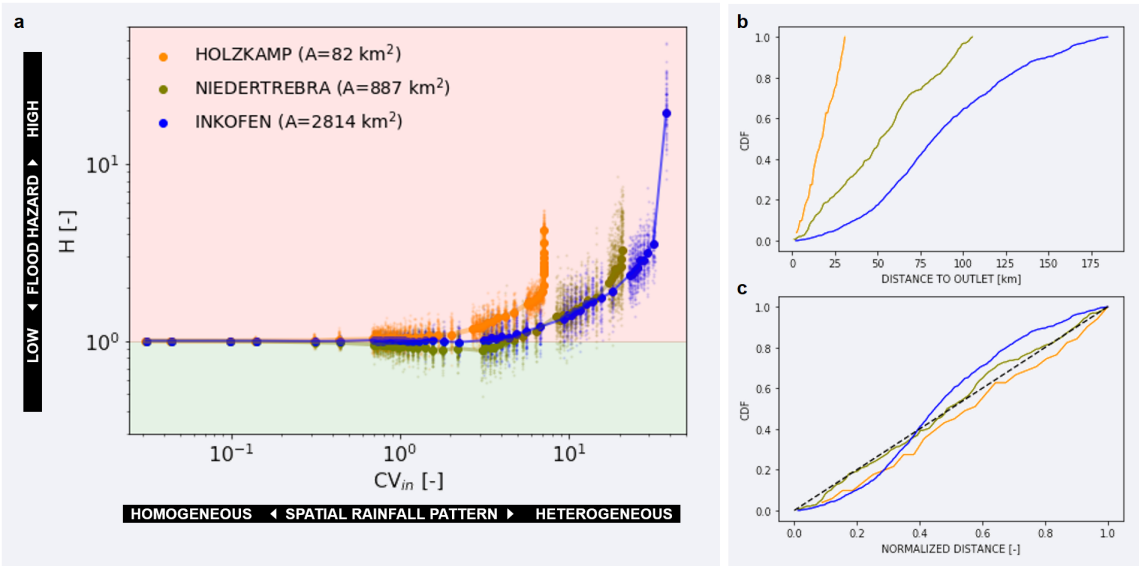

Figure 4. Effects of catchment size. Results for the Delme river basin at Holzkamp are displayed in orange color; results for the Ilm river basin at Niedertrebra are displayed in green color; results for the Amper river basin at Inkofen are displayed in blue color. (A) Effects of increasing spatial rainfall variability (CV_{in}) on the tail heaviness of streamflow distributions of catchments with increasing area. The red shaded area indicates heavier-tailed streamflow distributions with respect to the uniform rainfall case, whereas the green shaded area indicates lighter-tailed streamflow distributions. For each value of CV_{in} hundred different realizations of spatial rainfall patterns on the catchment characterized by the same spatial rainfall variability are displayed with small dots. The mean values of the tail heaviness among hundred results for each CV_{in} are displayed with large dots and linked with a tendency line. (B) Cumulative distribution function of runoff routing distance based on the DEM of each catchment. (C) Cumulative distribution function of runoff routing distance normalized with respect to the longest distance in each river network. The dash-black line is the 45-degree line which provides insights into the asymmetry (e.g., the skewness) of the distribution (indicated by the difference of area above and below the 45-degree line of the S-curve).

Catchment shape has been found to be related to the mainstream length (Sassolas-Serrayet et al., 2018) (i.e., the longest runoff routing distance). Therefore, in Figure 5 we investigate the effects of increasing spatial rainfall variability on the tail heaviness of streamflow distributions in catchments with different shapes. The Ilm river basin at Niedertrebra is more elongated (R_e = 0.45), the Innerste river basin at Heinde is less elongated (R_e = 0.78) and the Unstrut river basin at Erfurt-Moebisburg is circular (R_e = 0.90). Figure 5c displays their shapes. These catchments were selected because they have similar sizes (i.e., Niedertrebra: 887 km^2, Heinde: 898 km^2 and Erfurt-Moebisburg:

847 km^2) and drainage densities (i.e., $D_d < 1$ in all three catchments) to highlight the effect of catchment shape.

Figure 5a displays the comparison of responses of streamflow-distribution tail heaviness to spatial rainfall variability in these three catchments. For the more elongated catchment, tail heaviness of streamflow distributions increased when increasing of spatial rainfall variability above a certain threshold. However, for the less elongated and circular catchments, tail heaviness of streamflow distributions surprisingly is nearly independent to increasing spatial rainfall variability. To investigate the distinction of these catchments we plotted the cumulative distribution functions of normalized runoff routing distances in Figure 5b. Both the less elongated and circular catchments have clearly asymmetric runoff routing distance distributions, with more contributions from upstream than downstream catchment units. This finding confirms the previous discussion and suggests more catchment resilience to spatial rainfall variability may exist in circular catchments than elongated ones due to markedly asymmetric runoff routing distance distributions in circular catchments. However, this relationship may be further investigated by clarifying the role of catchment shape on the shape of runoff routing distance distribution.

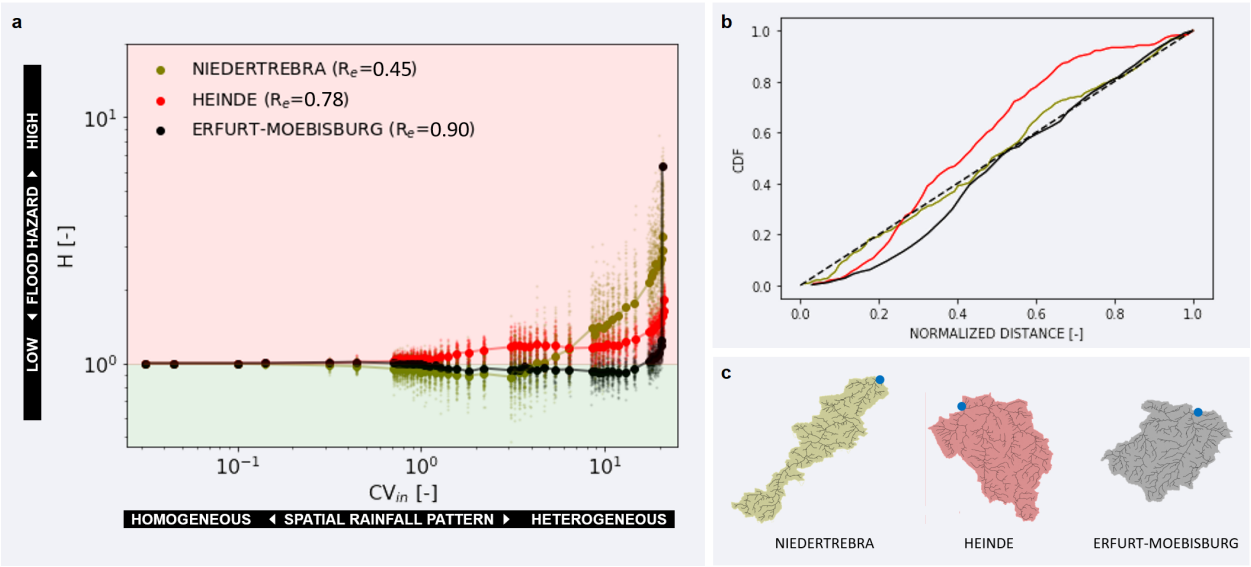

Figure 5. Effects of catchment shape. Results for the Ilm river basin at Niedertrebra (i.e., the more elongated catchment with $R_e = 0.45$) are displayed in green color; results for the Innerste river basin at Heinde (i.e., the less elongated catchment with $R_e = 0.78$) are displayed in red color; results for the Unstrut river basin at Erfurt-Moebisburg (i.e., the circular catchment with $R_e = 0.90$) are displayed in black color. (A) Effects of increasing spatial rainfall variability (CV_{in}) on the tail heaviness of streamflow distributions of catchments with different shapes. The red shaded area indicates heavier-tailed streamflow

distributions with respect to the uniform rainfall case, whereas the green shaded area indicates lighter-tailed streamflow distributions. For each value of CV_{in} hundred different realizations of spatial rainfall patterns on the catchment characterized by the same spatial rainfall variability are displayed with small dots. The mean values of the tail heaviness among hundred results for each CV_{in} are displayed with large dots and linked with a tendency line. (B) Cumulative distribution functions of runoff routing distance normalized with respect to the longest distance in each river network. The dash-black line is the 45-degree line (starting from the minimum and ending at the maximum of the S-Curve) which provides insights into the asymmetry (e.g., the skewness) of the distribution (indicated by the difference of area above and below the 45-degree line of the S-curve). (C) Visualization of the river networks and catchment shapes of the three catchments with the related color coding. Blue dots indicate the outlets of catchments.

4.3 Effects of Nonstationary Rainfall Variability

Figure 6 shows the response of the tail heaviness of streamflow distributions to increasing coefficient of variation of the spatial variability of rainfall across events (CV_{cross}). The red shaded area identifies cases with heavier tails than in the case of uniform rainfall. Results for catchments with different sizes and shapes are respectively displayed in Figure 6a, b. In Figure 6a, all three tendency lines show positive slopes which are significantly different from zero (Wald test with t-distribution, $p<0.05$). This indicates that the nonstationarity of spatial rainfall promotes an increase of the tail heaviness of streamflow distributions. The slope is significant ($p<0.05$) higher for the small ($= 0.71$) than the medium ($= 0.20$) and large ($= 0.09$) catchments. In Figure 6b, however, the slopes of the tendency lines of the less elongated (i.e., the red one) and circular (i.e., the black one) catchments are not significantly different from zero ($p \not< 0.05$). This means that nonstationarity has no effect on the streamflow distributions in these two catchments, which are comparatively more circular than the most elongated one. We recall that these results are consistent with the previous one, which suggested that smaller/elongated catchments are less resilient to increasing spatially heterogeneous rainfall. It is also worth to highlight that the impact from changing spatial variability of rainfall across events seems to be much less than the impact due to increasing spatial rainfall variability within the events.

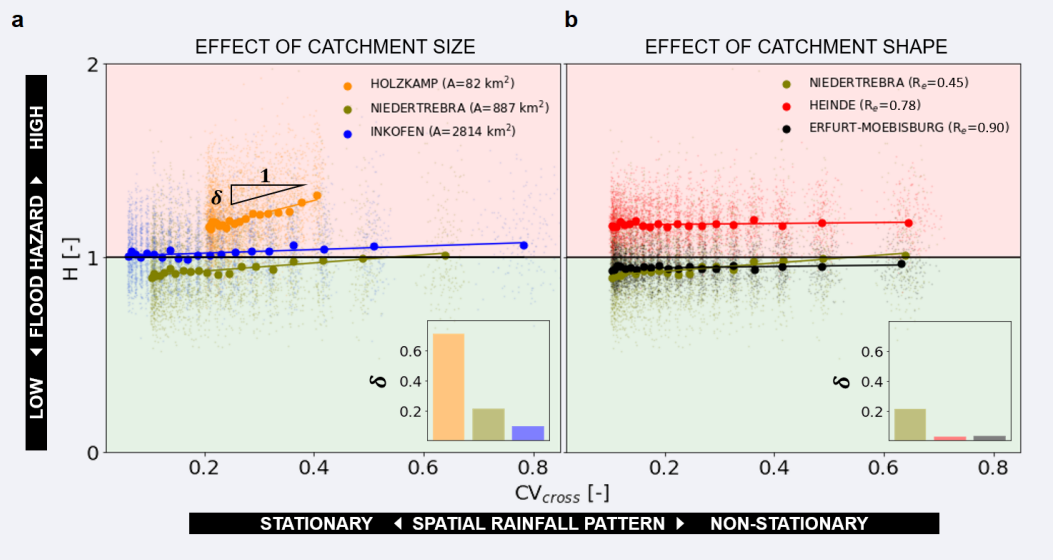

Figure 6. Effect of Nonstationarity of Spatial Rainfall (CV_{cross}). The red shaded area indicates heavier-tailed streamflow distributions with respect to the uniform rainfall case, whereas the green shaded area indicates lighter-tailed streamflow distributions. For each value of CV_{cross} hundred different realizations of spatial rainfall patterns on the catchment characterized by the same spatial rainfall variability are displayed with small dots. The mean values of the tail heaviness among hundred results for each CV_{cross} are displayed with large dots and linked with a tendency line. The slopes of the tendency lines are compared in the bar chart at the lower right corner of each panel. (A) Comparison of catchments with different sizes. (B) Comparison of catchments with different shapes.

4.4 Data Analyses

We analyzed relations in real data (although including the interlinked effect of rainfall, soil moisture, and river networks) to confirm the simulation results of the 5 select catchments and to prove the transferability of the synthetic results. The results in this section are based on the analysis of data for 175 catchments across Germany. Each dot in Figure 7 shows the slope and the correlation coefficient of a linear regression between the streamflow-distribution tail heaviness (H) and the average spatial rainfall variability (CV_{in}) for a single catchment. The slope value indicates the direction and magnitude of the relation between tail heaviness and spatial rainfall variability, whereas the correlation coefficient evaluates the reliability of this empirical relation. The area size of each catchment is displayed by the size of the dot. The slope of each regression was tested to be significantly ($p<0.05$) different from zero and catchments with significant slopes are shown in red, while slopes which are not significantly different from zero are shown in gray. In both Figure 7a and 7b we applied a single linear

regression for all values of spatial rainfall variability and estimated its significance. However, in Figure 7b, we also identified the threshold of CV_{in} beyond which an effect of increasing spatial rainfall variability begins to be visible (by means of the approach outlined in supporting information Text S2). All the catchments for which we identified such a threshold and thus display a certain resilience to increasing spatial rainfall variability are marked in purple color.

In general, more catchments (i.e., 102 out of 175) displayed positive than negative (73 out of 175) relations between spatial rainfall variability and tail heaviness. All the negative cases displayed weak relations (i.e., closed-to-zero slopes). In Figure 7a, 37 of 102 catchments (i.e., 36%) displayed significant positive slopes whereas only 9 of 73 catchments (i.e., 12%) showed significant negative slopes. These results confirmed what we found in simulations, i.e., that increasing spatial variability of rainfall mostly determines heavier streamflow-distribution tails. It is worth noting that among all significant catchments in Figure 7a, large catchments displayed weaker relations (i.e., lower slopes) whereas small catchments displayed stronger relations (i.e., higher slopes). This confirms the existence of more resilience to spatial rainfall in large catchments than in small ones identified by means of simulation analyses.

In Figure 7b, 48 catchments for which we identified either significant-positive slopes (shown in red) or an effective threshold of average spatial rainfall variability (shown in purple) are displayed. All of the large catchments (> 1000 km^2) among them are the latter case (i.e., shown in purple), in agreement with the findings of our simulations according to which large catchments are more resilient to spatial rainfall variability and therefore only display increasing tail heaviness of streamflow distribution beyond a threshold of spatial rainfall variability.

However, it should be noticed that these results came from mixed effects of both intra- and cross-event variability of spatial rainfall because there are still variations of spatial rainfall variability from event to event in each rainfall-runoff group. Both the linear regressions and the streamflow distributions were computed from limited data, which likely influenced the reliability of these correlations in some cases. Nevertheless, the results of the data analysis align and confirm the simulation results.

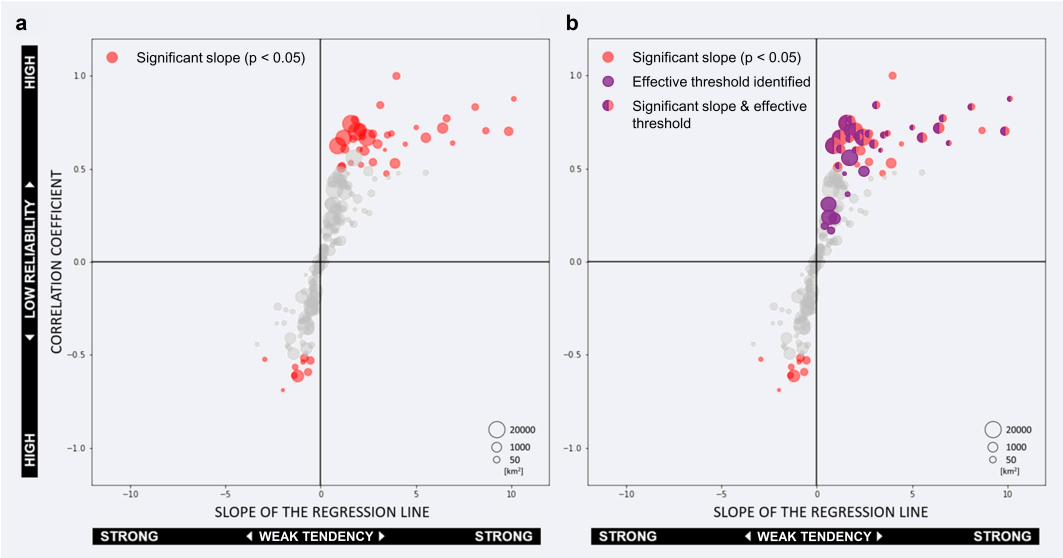

Figure 7. Data-based linear regressions between streamflow-distribution tail heaviness and average spatial rainfall variability. Results for 175 catchments in Germany are displayed with their areas represented by the sizes of dots. Each dot shows the slope and the correlation coefficient of a linear regression between the streamflow-distribution tail heaviness and the average spatial rainfall variability for a single catchment. The slope value indicates the direction and magnitude of the relation between tail heaviness and spatial rainfall variability, whereas the correlation coefficient evaluates the reliability of this empirical relation. (A) Evaluation of the linear correlation between streamflow-distribution tail heaviness and average spatial rainfall variability. Red dots indicated the catchments whose slopes were significant greater/less than zero at a 0.05 significance level; gray dots indicated the catchments whose slopes were not significantly different from zero. (B) Identification of a threshold beyond which an effect of increasing spatial rainfall variability begins to be visible. Purple dots indicate catchments for which a minimum threshold of spatial rainfall variability for seeing an effect on tail heaviness was identified; red dots indicate catchments for which a linear regression between spatial rainfall variability and tail heaviness (i.e., disregarding the threshold) had slope significantly different from zero; gray dots shown all the other catchments where such relations were not significant.

1. Summary and Conclusions

In this study, we addressed the impacts of spatial rainfall variability on the increasing hazard of high flows. We synthetically generated spatially variable rainfall in two scenarios: stationary (i.e., constant spatial rainfall variability across events) and nonstationary (i.e., variable spatial rainfall variability across events). A continuous probabilistic model of water transport at the catchment

scale was used to simulate the hydrological response. The effects of spatial rainfall variability on the tail heaviness of streamflow distributions were investigated in five select catchments under different spatial rainfall scenarios (i.e., stationary and nonstationary), catchment sizes (i.e., small, medium, large), and catchment shapes (i.e., more elongated, less elongated, circular). Furthermore, we analyzed the relation between spatial rainfall variability and tail heaviness of streamflow distributions by using recorded data from 175 river catchments to validate the simulation results and test their transferability. The key conclusions of the study are:

1. Increasing spatial variability of rainfall determines enhanced hazard of high flows (i.e., heavier tails of flow distributions) only beyond a certain increase threshold. Both the value of this threshold and the growth rate of tail heaviness beyond the threshold indicate the resilience of catchments to spatially variable rainfall.

2. Small or elongated catchments show less resilience to increasing spatial variability of rainfall compared to large or circular catchments. High asymmetry of the distribution of runoff routing distances along river networks identified for large and circular catchments (with more contributions from upstream than downstream catchment units) is likely to provide more resilience to increasing spatial variability of rainfall.

3. In line with the previous results, smaller or more elongated catchments are more influenced by the nonstationarity of the spatial variability of rainfall across events. However, this nonstationarity seems to influence less the tail of streamflow distributions than the spatial variability of rainfall during the event.

4. Analyses of daily rainfall-runoff records for a large set of catchments in Germany agree with the simulation results, showing positive correlations between spatial rainfall variability and streamflow-distribution tail heaviness in the majority of the case studies. Data analyses also confirm that large catchments are more resilient to increasing spatial rainfall variability, as previously found by means of synthetic simulations.

This work pinpoints the role played by the spatial heterogeneity of rainfall for controlling the emergence of heavy-tailed distributions of streamflow. It thus establishes a link between expected alterations of rainfall caused by the ongoing climate change, such as more localized rain, and the resulting modifications in the frequency of large event magnitudes, with implications for the hazard of high flows in different river basins.

Acknowledgments

This work is funded by the Deutsche Forschungsgemeinschaft (DFG, German Research Foundation) - Project number 421396820 “Propensity of rivers to extreme floods: climate-landscape controls and early detection (PREDICTED)” and Research Group FOR 2416 “Space-Time Dynamics of Extreme Floods (SPATE)”.

The financial support of the Helmholtz Centre for Environmental Research - UFZ is as well acknowledged. The first author is also thankful to the Ministry of Education of the Republic of China (Taiwan) (MOE) for providing financial support to this study (GSSA-2020SG12). SY (the 3rd author) acknowledges the support of the Helmholtz Climate Initiative Project funded by the Helmholtz Association. The manuscript and supporting information provide all the information needed to replicate the results.

Data Availability Statement

For providing the discharge data for Germany, we are grateful to the Bavarian State Office of Environment (LfU, https://www.gkd.bayern.de/de/fluesse/abfluss) and Global Runoff Data Centre (GRDC) prepared by the Federal Institute for Hydrology (BfG, http://www.bafg.de/GRDC). Climatic data can be obtained from the German Weather Service (DWD; ftp://ftp-cdc.dwd.de/pub/CDC/). Digital elevation model can be retrieved from Shuttle Radar Topography Mission (SRTM; http://www.cgiar-csi.org/data/srtm-90m-digital-elevation-database-v4-1). Land use data are available from the Copernicus monitoring system (http://land.copernicus.eu/pan-european/corine-landcover). Characteristics of separated rainfall-runoff events for every streamflow gauge used in the analysis can be found in Data Set S1 of Tarasova et al., 2018 (https://doi.org/10.1029/2018WR022588).

References

Ács, F., Horváth, Á., Breuer, H., & Rubel, F. (2010). Effect of soil hydraulic parameters on the local convective precipitation. *Meteorologische Zeitschrift*, *19*(2), 143–153. https://doi.org/10.1127/0941-2948/2010/0435

Adhikari, S. (2020). Morphometric Analysis of a Drainage Basin: A Study of Ghatganga River, Bajhang District, Nepal. *The Geographic Base*, *7*, 127–144. https://doi.org/10.3126/tgb.v7i0.34280

Allard, D., & Soubeyrand, S. (2012). Skew-normality for climatic data and dispersal models for plant epidemiology: When application fields drive spatial statistics. *Spatial Statistics*, *1*, 50–64. https://doi.org/10.1016/j.spasta.2012.03.001

Arnell, N. W., & Gosling, S. N. (2016). The impacts of climate change on river flood risk at the global scale. *Climatic Change*, *134*(3), 387–401. https://doi.org/10.1007/s10584-014-1084-5

Ayalew, T. B., Krajewski, W. F., & Mantilla, R. (2014). Connecting the power-law scaling structure of peak-discharges to spatially variable rainfall and catchment physical properties. *Advances in Water Resources*, *71*, 32–43. https://doi.org/10.1016/j.advwatres.2014.05.009

Basso, S., Schirmer, M., & Botter, G. (2016). A physically based analytical model of flood frequency curves. *Geophysical Research Letters*, *43*(17), 9070–9076. https://doi.org/10.1002/2016GL069915

Basso, S., Schirmer, M., & Botter, G. (2015). On the emergence of heavy-tailed streamflow distributions. *Advances in Water Resources*, *82*, 98–105. https://doi.org/10.1016/j.advwatres.2015.04.013

Ben-Gai, T., Bitan, A., Manes, A., Alpert, P., & Rubin, S. (1998). Spatial and temporal changes in rainfall frequency distribution patterns in Israel. *Theoretical and Applied Climatology*, *61*(3–4), 177–190. https://doi.org/10.1007/s007040050062

Beurton, S., & Thieken, A. H. (2009). Seasonality of floods in Germany. *Hydrological Sciences Journal*, *54*(1), 62–76. https://doi.org/10.1623/hysj.54.1.62

Borga, M., Boscolo, P., Zanon, F., & Sangati, M. (2007). Hydrometeorological analysis of the 29 August 2003 flash flood in the eastern Italian Alps. *Journal of Hydrometeorology*, *8*(5), 1049–1067. https://doi.org/10.1175/JHM593.1

Bowers, M. C., Tung, W. W., & Gao, J. B. (2012). On the distributions of seasonal river flows: Lognormal or power law? *Water Resources Research*, *48*(5), 1–12. https://doi.org/10.1029/2011WR011308

Boyd, M. J. (1978). A storage-routing model relating drainage basin hy- drology and geomorphology. *Water Resources Research*, *14*(5), 921–928.

Bracken, L., Cox, N., & Shannon, J. (2008). The relationship between rainfall inputs an flood generation in south-east Spain. *Hydrological Processes*, *22*(5). https://doi.org/10.1002/hyp.6641

Clapp, R. B., & Hornberger, G. M. (1978). Empirical equations for some soil hydraulic properties. *Water Resources Research*, *14*(4), 601–604.

Clauset, A., Shalizi, C. R., & Newman, M. E. J. (2009). Power-law distributions in empirical data. *SIAM Review*, *51*(4), 661–703. https://doi.org/10.1137/070710111

Clauset, A., Young, M., & Gleditsch, K. S. (2007). On the frequency of severe terrorist events. *Journal of Conflict Resolution*, *51*(1), 58–87. https://doi.org/10.1177/0022002706296157

Darras, T., Borrell Estupina, V., Kong-A-Siou, L., Vayssade, B., Johannet, A., & Pistre, S. (2015). Identification of spatial and temporal contributions of rainfalls to flash floods using neural network modelling: Case study on the Lez basin (southern France). *Hydrology and Earth System Sciences*, *19*(10), 4397–4410. https://doi.org/10.5194/hess-19-4397-2015

D'Odorico, P., & Rigon, R. (2003). Hillslope and channel contributions to the hydrologic response. *Water Resources Research*, *39*(5), 1–9. https://doi.org/10.1029/2002WR001708

Donat, M. G., Angélil, O., & Ukkola, A. M. (2019). Intensification of precipitation extremes in the world's humid and water-limited regions. *Environmental Research Letters*, *14*(6). https://doi.org/10.1088/1748-9326/ab1c8e

Donat, M. G., Lowry, A. L., Alexander, L. V., O'Gorman, P. A., & Maher, N. (2016). More extreme precipitation in the worldâ €$^{\mathrm{TM}}$ s dry and wet regions. *Nature Climate Change*, *6*(5), 508–513. https://doi.org/10.1038/nclimate2941

El Adlouni, S., Bobée, B., & Ouarda, T. B. M. J. (2008). On the tails of extreme event distributions in hydrology. *Journal of Hydrology*, *355*(1–4), 16–33. https://doi.org/10.1016/j.jhydrol.2008.02.011

ESRI. (2009). Arc Hydro Tools - Tutorial. *New York*, (January), 136.

Gaetan, C., & Grigoletto, M. (2007). A hierarchical model for the analysis of spatial rainfall extremes. *Journal of Agricultural, Biological, and Environmental Statistics*, *12*(4), 434–449. https://doi.org/10.1198/108571107X250193

Gioia, A., Iacobellis, V., Manfreda, S., & Fiorentino, M. (2008). Runoff thresholds in derived flood frequency distributions. *Hydrology and Earth System Sciences*, *12*(6), 1295–1307. https://doi.org/10.5194/hess-12-1295-2008

Gupta, V. K., & Waymire, E. C. (1998). Spatial Variability and Scale Invariance in Hydrologic Regionalization. In G. Sposito (Ed.), *Scale Dependence and Scale Invariance in Hydrology* (pp. 88–135). Cambridge University Press. https://doi.org/https://doi.org/10.1017/CBO9780511551864.005

Harman, C. J., Sivapalan, M., & Kumar, P. (2009). Power law catchment-scale recessions arising from heterogeneous linear small-scale dynamics. *Water Resources Research*, *45*(9), 1–13. https://doi.org/10.1029/2008WR007392

Horton, R. E. (1945). Erosional development of streams and their drainage basins: hydro-physical approach to quantitative morphology. *Geological Society of America Bulletin*, *56*(3), 275–370. https://doi.org/doi:10.1130/0016-7606(1945)56[275:EDOSAT]2.0.CO;2

Horton, R. E. (1932). Drainage-basin characteristics. *Transactions of the American Geophysical Union*, *13*(1), 350–361. https://doi.org/10.1029/TR013i001p00350

Houska, T., Kraft, P., Chamorro-Chavez, A., & Breuer, L. (2015). SPOTting model parameters using a ready-made python package. *PLoS ONE*, *10*(12), 1–22. https://doi.org/10.1371/journal.pone.0145180

Hu, Q., Li, Z., Wang, L., Huang, Y., Wang, Y., & Li, L. (2019). Rainfall spatial estimations: A review from spatial interpolation to multi-source data merging. *Water (Switzerland)*, *11*(3), 1–30. https://doi.org/10.3390/w11030579

Hughes, D. A., & Smakhtin, V. (1996). Daily flow time series patching or extension: a spatial interpolation approach based on flow duration curves. *Hydrological Sciences Journal*, *41*(6), 851–871. https://doi.org/10.1080/02626669609491555

Kale, V. S., & Gupta, A. (2001). *Introduction to Geomorphology*. New Delhi: Orient Longman.

Katz, R. W., Parlange, M. B., & Naveau, P. (2002). Statistics of extremes in hydrology. *Advances in Water Resources*, *25*(8–12), 1287–1304.

https://doi.org/10.1016/S0309-1708(02)00056-8

Kirkby, M. (1975). Hydrograph modelling strategies, in Processes in Human and Physical Geography. In R. Peel, M. Chisholm, & P. Haggett (Eds.) (pp. 69–90). London: Heinemann.

Kumar, R., Chatterjee, C., Singh, R. D., Lohani, A. K., & Kumar, S. (2007). Runoff estimation for an ungauged catchment using geomorphological instantaneous unit hydrograph (GIUM) models. *Hydrological Processes*, *21*(14), 1829–1840. https://doi.org/10.1002/hyp.6318

Lehner, B., Liermann, C. R., Revenga, C., Vörömsmarty, C., Fekete, B., Crouzet, P., et al. (2011). High-resolution mapping of the world's reservoirs and dams for sustainable river-flow management. *Frontiers in Ecology and the Environment*, *9*(9), 494–502. https://doi.org/10.1890/100125

Li, C., Zwiers, F., Zhang, X., Chen, G., Lu, J., Li, G., et al. (2019). Larger Increases in More Extreme Local Precipitation Events as Climate Warms. *Geophysical Research Letters*, *46*(12), 6885–6891. https://doi.org/10.1029/2019GL082908

Li, Z., Brissette, F., & Chen, J. (2014). Assessing the applicability of six precipitation probability distribution models on the Loess Plateau of China. *International Journal of Climatology*, *34*(2), 462–471. https://doi.org/10.1002/joc.3699

Li, Z., & Shi, X. (2019). Stochastic generation of daily precipitation considering diverse model complexity and climates. *Theoretical and Applied Climatology*, *137*(1–2), 839–853. https://doi.org/10.1007/s00704-018-2638-7

Lu, P., Smith, J. A., & Lin, N. (2017). Spatial characterization of flood magnitudes over the drainage network of the Delaware river basin. *Journal of Hydrometeorology*, *18*(4), 957–976. https://doi.org/10.1175/JHM-D-16-0071.1

Marchi, L., Borga, M., Preciso, E., & Gaume, E. (2010). Characterisation of selected extreme flash floods in Europe and implications for flood risk management. *Journal of Hydrology*, *394*(1–2), 118–133. https://doi.org/10.1016/j.jhydrol.2010.07.017

Menabde, M., & Sivapalan, M. (2001). Linking space-time variability of river runoff and rainfall fields: A dynamic approach. *Advances in Water Resources*, *24*(9–10), 1001–1014. https://doi.org/10.1016/S0309-1708(01)00038-0

Merz, R., & Blöschl, G. (2009). Process controls on the statistical flood moments - a data based analysis. *Hydrological Processes*, *23*(5), 675–696. https://doi.org/10.1002/hyp

Myhre, G., Alterskjær, K., Stjern, C. W., Hodnebrog, Marelle, L., Samset, B. H., et al. (2019). Frequency of extreme precipitation increases extensively with event rareness under global warming. *Scientific Reports*, *9*(1), 1–10. https://doi.org/10.1038/s41598-019-52277-4

Nag, S. K., & Chakraborty, S. (2003). Influence of rock types and structures in the development of drainage network in hard rock area. *Journal of the Indian*

Society of Remote Sensing, *31*(1), 25–35. https://doi.org/10.1007/bf03030749

Nerantzaki, S. D., & Papalexiou, S. M. (2019). Tails of extremes: Advancing a graphical method and harnessing big data to assess precipitation extremes. *Advances in Water Resources*, *134*. https://doi.org/10.1016/j.advwatres.2019.103448

Ng, J. L., Abd Aziz, S., Huang, Y. F., Wayayok, A., & Rowshon, M. (2018). Generation of a stochastic precipitation model for the tropical climate. *Theoretical and Applied Climatology*, *133*(1–2), 489–509. https://doi.org/10.1007/s00704-017-2202-x

Nicótina, L., Alessi Celegon, E., Rinaldo, A., & Marani, M. (2008). On the impact of rainfall patterns on the hydrologic response. *Water Resources Research*, *44*(12), 1–14. https://doi.org/10.1029/2007WR006654

Papalexiou, S. M., & Serinaldi, F. (2020). Random Fields Simplified: Preserving Marginal Distributions, Correlations, and Intermittency, With Applications From Rainfall to Humidity. *Water Resources Research*, *56*(2). https://doi.org/10.1029/2019WR026331

Park, S.-Y. (2014). Prediction of direct runoff hydrographs utilizing stochastic network models: a case study in South Korea. *Hydrology and Earth System Sciences Discussions*, *11*(10), 11247–11279. https://doi.org/10.5194/hessd-11-11247-2014

Paschalis, A., Fatichi, S., Molnar, P., Rimkus, S., & Burlando, P. (2014). On the effects of small scale space-time variability of rainfall on basin flood response. *Journal of Hydrology*, *514*, 313–327. https://doi.org/10.1016/j.jhydrol.2014.04.014

Peleg, N., Blumensaat, F., Molnar, P., Fatichi, S., & Burlando, P. (2017). Partitioning the impacts of spatial and climatological rainfall variability in urban drainage modeling. *Hydrology and Earth System Sciences*, *21*(3), 1559–1572. https://doi.org/10.5194/hess-21-1559-2017

Pendergrass, A. G. (2018). What precipitation is extreme? *Science*, *360*(6393), 1072–1073. https://doi.org/10.1126/science.aat1871

Rauthe, M., Steiner, H., Riediger, U., Mazurkiewicz, A., & Gratzki, A. (2013). A Central European precipitation climatology - Part I: Generation and validation of a high-resolution gridded daily data set (HYRAS). *Meteorologische Zeitschrift*, *22*(3), 235–256. https://doi.org/10.1127/0941-2948/2013/0436

Rigon, R., Bancheri, M., Formetta, G., & deLavenne, A. (2016). The geomorphological unit hydrograph from a historical-critical perspective. *Earth Surface Processes and Landforms*, *41*(1), 27–37. https://doi.org/10.1002/esp.3855

Rinaldo, A., Botter, G., Bertuzzo, E., Uccelli, A., Settin, T., & Marani, M. (2006). Transport at basin scales: 1. Theoretical framework. *Hydrology and Earth System Sciences*, *10*(1), 19–29. https://doi.org/10.5194/hess-10-19-2006

Rinaldo, A., Marani, A., & Rigon, R. (1991). Geomorphological dispersion. *Water Resources Research*, *27*(4), 513–525. https://doi.org/10.1029/90WR02501

Rinaldo, A., & Rodriguez-Iturbe, I. (1996). Geomorphological theory of the hydrological response. *Hydrological Processes*, *10*(6), 803–829. https://doi.org/10.1002/(SICI)1099-1085(199606)10:6<803::AID-HYP373>3.0.CO;2-N

Rodríguez-Iturbe, I., & Valdés, J. B. (1979). The geomorphologic structure of hydrologic response. *Water Resources Research*, *15*(6), 1409–1420. https://doi.org/10.1029/WR015i006p01409

Rogger, M., Kohl, B., Pirkl, H., Viglione, A., Komma, J., Kirnbauer, R., et al. (2012). Runoff models and flood frequency statistics for design flood estimation in Austria - Do they tell a consistent story? *Journal of Hydrology*, *456–457*, 30–43. https://doi.org/10.1016/j.jhydrol.2012.05.068

Sassolas-Serrayet, T., Cattin, R., & Ferry, M. (2018). The shape of watersheds. *Nature Communications*, *9*(1), 1–8. https://doi.org/10.1038/s41467-018-06210-4

Schumm, S. A. (1956). Evolution of drainage systems and slopes in Badlands at Perth Amboy, New Jersey. *Geological Society of America Bulletin*, *67*, 597–646.

Sharma, A., Wasko, C., & Lettenmaier, D. P. (2018). If Precipitation Extremes Are Increasing, Why Aren't Floods? *Water Resources Research*, *54*(11), 8545–8551. https://doi.org/10.1029/2018WR023749

Singh, V. P. (1997). Effect of spatial and temporal variability in rainfall and watershed characteristics on stream flow hydrograph. *Hydrological Processes*, *11*, 1649–1669.

Sivapalan, M., Blöschl, G., Merz, R., & Gutknecht, D. (2005). Linking flood frequency to long-term water balance: Incorporating effects of seasonality. *Water Resources Research*, *41*(6), 1–17. https://doi.org/10.1029/2004WR003439

Strahler, A. N. (1952). Hypsometric (area-altitude) analysis of erosional topology. *Geological Society of America Bulletin*, *63*(11), 1117–1142. https://doi.org/doi:10.1130/0016-7606(1952)63[1117:HAAOET]2.0.CO;2

Strahler, A. N. (1957). Quantitative analysis of watershed geomorphology. *Transactions of the American Geophysical Union*, *38*(6), 913–920. https://doi.org/doi:10.1029/tr038i006p00913

Strahler, A. N. (1964). Quantitative geomorphology of drainage basins and channel networks. In *Chow by VenTe (ed) Handbook of applied hydrology*. New York: McGraw Hill Book Company.

Struthers, I., & Sivapalan, M. (2007). A conceptual investigation of process controls upon flood frequency: Role of thresholds. *Hydrology and Earth System Sciences*, *11*(4), 1405–1416. https://doi.org/10.5194/hess-11-1405-2007

Tabari, H. (2020). Climate change impact on flood and extreme precipitation increases with water availability. *Scientific Reports*, *10*(1), 1–10. https://doi.org/10.1038/s41598-020-70816-2

Taleb, N. N. (2007). *The black swan: The impact of the highly improbable*. New York: Random House. https://doi.org/10.4324/9781912281206

Tarasova, L., Basso, S., Zink, M., & Merz, R. (2018). Exploring Controls on Rainfall-Runoff Events: 1. Time Series-Based Event Separation and Temporal Dynamics of Event Runoff Response in Germany. *Water Resources Research*, *54*(10), 7711–7732. https://doi.org/10.1029/2018WR022587

Thornthwaite, C. W. (1948). An Approach toward a Rational Classification of Climate. *Geographical Review*, *38*(1), 55. https://doi.org/10.2307/210739

Viglione, A., Chirico, G. B., Woods, R., & Blöschl, G. (2010). Generalised synthesis of space-time variability in flood response: An analytical framework. *Journal of Hydrology*, *394*(1–2), 198–212. https://doi.org/10.1016/j.jhydrol.2010.05.047

Villarini, G., & Smith, J. A. (2010). Flood peak distributions for the eastern United States. *Water Resources Research*, *46*(6), 1–17. https://doi.org/10.1029/2009WR008395

Vogel, R. M., & Fennessey, N. M. (1994). Flow-duration curves I: new interpretation and confidence intervals. *Journal of Water Resources Planning and Management*, *120*(4), 485–504. https://doi.org/doi. org/10.1061/(ASCE)0733-9496(1994)120:4(485)

Wasko, C., & Sharma, A. (2017). Global assessment of flood and storm extremes with increased temperatures. *Scientific Reports*, *7*(1), 1–8. https://doi.org/10.1038/s41598-017-08481-1

Wietzke, L. M., Merz, B., Gerlitz, L., Kreibich, H., Guse, B., Castellarin, A., & Vorogushyn, S. (2020). Comparative analysis of scalar upper tail indicators. *Hydrological Sciences Journal*, *65*(10), 1625–1639. https://doi.org/10.1080/02626667.2020.1769104

Withanage, N. S., Dayawansa, N. D. K., & De Silva, R. P. (2014). Morphometric analysis of the Gal Oya river basin using spatial data derived from GIS. *Tropical Agricultural Research*, *26*(1), 175–188. https://doi.org/10.4038/tar.v26i1.8082

Woltemade, C. J., & Potter, K. W. (1994). A watershed modeling analysis of fluvial geomorphic influences on flood peak attenuation. *Water Resources Research*, *30*(6), 1933–1942.

Yang, S., Paik, K., McGrath, G. S., Urich, C., Krueger, E., & Kumar, P., & Rao, P. S. C. (2017). Functional topology of evolving urban drainage networks. *Water Resources Research*, *53*, 8966–8979. https://doi.org/https://doi.org/10.1002/2017WR021555

Ye, L., Hanson, L. S., Ding, P., Wang, D., & Vogel, R. M. (2018). The probability distribution of daily precipitation at the point and catchment scales in the United States. *Hydrology and Earth System Sciences*, *22*(12), 6519–6531. https://doi.org/10.5194/hess-22-6519-2018

Yokoo, Y., & Sivapalan, M. (2011). Towards reconstruction of the flow duration curve: Development of a conceptual framework with a physical basis. *Hydrology and Earth System Sciences*, *15*(9), 2805–2819. https://doi.org/10.5194/hess-15-2805-2011

Zhao, F., Zhang, L., Chiew, F. H. S., Vaze, J., & Cheng, L. (2013). The effect of spatial rainfall variability on water balance modelling for south-eastern Australian catchments. *Journal of Hydrology*, *493*, 16–29. https://doi.org/10.1016/j.jhydrol.2013.04.028

Zhu, Z., Wright, D. B., & Yu, G. (2018). The Impact of Rainfall Space-Time Structure in Flood Frequency Analysis. *Water Resources Research*, *54*(11), 8983–8998. https://doi.org/10.1029/2018WR023550

Zink, M., Kumar, R., Cuntz, M., & Samaniego, L. (2017). A high-resolution dataset of water fluxes and states for Germany accounting for parametric uncertainty. *Hydrology and Earth System Sciences*, *21*(3), 1769–1790. https://doi.org/10.5194/hess-21-1769-2017

Zoccatelli, D., Borga, M., Viglione, A., Chirico, G. B., & Blöschl, G. (2011). Spatial moments of catchment rainfall: Rainfall spatial organisation, basin morphology, and flood response. *Hydrology and Earth System Sciences*, *15*(12), 3767–3783. https://doi.org/10.5194/hess-15-3767-2011